Sunan Kalijaga of Journal Physics
Vol. 7, No. 1, 2025, pp. 31-41
ISSN: 2715-0402, DOI: https://doi.org/10.14421/physics.v7i1.5637

Subsurface Structure Analysis for Determining the Slip Surface of Landslides Using the Wenner Resistivity Geoelectrical Method in Kokap, Kulon Progo

Rezal Prihatin[1*], Thaqibul Fikri Niyartama[2]
[1,2] Departement of Physics, Sunan Kalijaga State Islamic University. Yogyakarta, Indonesia
[*]freehatin99@gmail.com

ARTICLE INFO

Article history:

Received February 22, 2025
Revised March 25, 2025
Accepted April 23, 2025

Keywords:

Geophysical investigation
Resistivity method
Subsurface profile
Andesitic slope

ABSTRACT

Slope failures frequently occur in hilly regions, particularly during periods of intense rainfall. At the end of 2022, such an event affected a residential area in Hargomulyo Village, Kulon Progo. Mitigation efforts against similar hazards can be implemented through mapping of landslide-prone zones, one of which involves identifying the rock layers that act as the slip surface. This study employs the geoelectrical resistivity method with a Wenner configuration to characterize the subsurface structure based on variations in electrical resistivity of soil and rock. Data acquisition was conducted along four survey lines located within an andesitic intrusion formation composed of hypersthene–andesite to trachyandesite rocks. The modeling results indicate three main layers: surface soil with resistivity values below 54.4 Ωm, clay mixed with weathered andesite ranging from 54.4 Ωm to 141 Ωm, and intact andesite bedrock exceeding 141 Ωm. Correlation with the Geological Map of Yogyakarta Sheet (Rahardjo et al., 1995) confirms that the potential slip surface corresponds to the weathered andesite–clay zone developed along the contact between the Andesite Intrusion and the Kebobutak Formation. This transition layer, acting as a mechanically weak zone, controls slope stability in the study area. The presence of a local north–south fault may further increase groundwater infiltration and pore pressure above the impermeable andesite layer, promoting slope movement during heavy rainfall. These results emphasize that integrating resistivity interpretation with geological mapping provides a more comprehensive understanding of landslide mechanisms and supports hazard mitigation efforts in andesitic terrains of Kulon Progo.

Cite Article:

R. Prihatin, T. F. Niyartama, "Subsurface Structure Analysis for Determining the Slip Surface of Landslides Using the Wenner Resistivity Geoelectrical Method in Kokap, Kulon Progo," in *Sunan Kalijaga of Journal Physics*, vol. 7, no. 1, pp. 31-40. April, 2025, 10.14421/physics.v7i1.5637.

1. INTRODUCTION

Slope failures are among the most frequent natural hazards occurring in hilly regions with steep slopes, particularly during the rainy season. One of the areas characterized by such steep terrain is the Menoreh Mountains, located in the western part of the Special Region of Yogyakarta Province. According to a report

by detik.com [3], a 15-meter-high cliff collapsed, striking one house and two motorcycles. Heavy rainfall occurred on the afternoon of Monday, November 8, 2023, shortly before the incident. The Regional Disaster Management Agency (BPBD) of Kulon Progo recorded at least 42 landslide occurrences during that period of intense rainfall. These events were distributed across the districts of Girimulyo, Kokap, and Pengasih.

A landslide is defined as the downslope movement of soil mass, rock, or a combination of both due to a loss of slope stability [13]. Such events are common in tropical regions like Indonesia [26]. Several factors influence slope failure, including slope gradient, rainfall intensity, and the physical characteristics of the soil or rock that constitute the slip surface. The slip surface refers to the layer that acts as the movement plane for the sliding material [5]. Hence, identifying the layer that serves as the slip surface is essential for assessing and mapping landslide potential [21].

One of the effective techniques for mapping the slip surface is the geoelectrical resistivity method [18]. This method operates on the principle of injecting an electric current into the ground and measuring the resulting potential difference. The measured potential difference is then used to calculate the subsurface resistivity, which helps classify subsurface materials, including those forming the potential slip surface. The resistivity method can be implemented using several electrode configurations, such as Wenner, Schlumberger, and Dipole–Dipole arrays.

The Wenner configuration is commonly used for lateral subsurface mapping. In this configuration, the electrodes are spaced at equal distances. It provides a model with high horizontal resolution but limited depth penetration [6]. The choice of configuration in a resistivity survey depends on the research objective. For identifying the slip surface, a configuration capable of resolving the lateral variations of subsurface rock layers is required. Therefore, this study employs the Wenner configuration, which is well-suited for generating high-resolution horizontal models of subsurface structures.

1.1. Geological Conditions of Hargomulyo Area

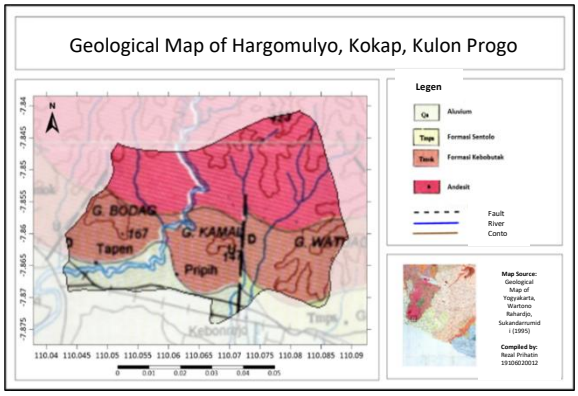

Figure 1. Geological Map of Hargomulyo

The study area, located in Hargomulyo Area, Kapanewon Kokap, Kulon Progo Regency, lies at the southern edge of the Menoreh Mountains — a mountain range stretching from the southern part of Borobudur Temple in Magelang Regency to the southern coast of Kulon Progo Regency. This area consists of hilly terrain with steep slopes. There is also a river flowing from north to south, eventually discharging into the Indian Ocean.

Hargomulyo Area is composed of four geological formations [16]. In the northern part lies an Andesite intrusion composed of hypersthene-andesite to augite-hornblende and trachyandesite. Approximately half of the northern section of Hargomulyo Area is made up of this Andesite intrusion, represented in Figure 1. The remaining northern section is dominated by the Kebobutak Formation. This formation consists of alternating sedimentary and volcanic rocks composed of andesitic breccia, tuff, lapilli tuff, agglomerate, and intercalations of andesitic lava flows. In Figure 1, the Kebobutak Formation is shown in a reddish-brown color.

In the southwestern part, a small portion consists of surface deposits of Alluvium. The Alluvium comprises gravel, silt, sand, and clay deposits along major rivers and coastal plains. The Sentolo Formation, composed of limestone and marly sandstone, appears only in a very small section in the southeastern part of Hargomulyo Area. Additionally, there is a local fault running from the central to the southern part of the village. This fault crosses three geological formations — the Andesite intrusion, the Kebobutak Formation, and the Alluvium deposits.

1.2. Topographic Profile of Hargomulyo Area

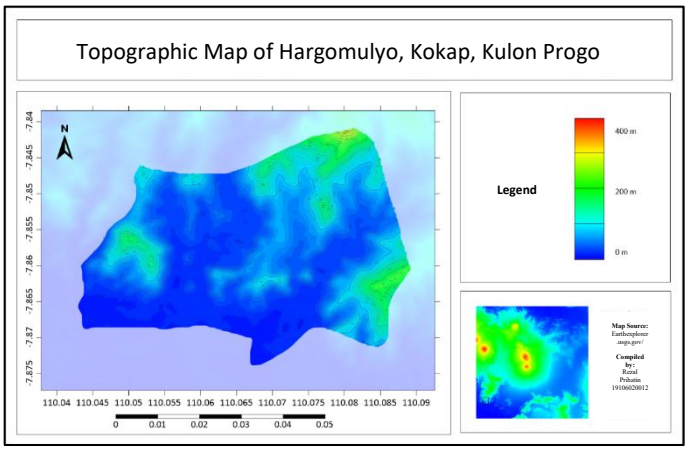

Figure 2. Topographical Map of Hargomulyo

Hargomulyo Area is located at the southern tip of the Menoreh Mountains. The area exhibits a diverse elevation range from 20 meters to 320 meters above sea level (masl), as shown in Figure 2. The majority of the region consists of plains with elevations between 20 and 40 masl, represented in Figure 2 by the blue color.

The lowest point lies in the southern part, with an elevation of 20 masl, shown in blue on Figure 2. The highest point is located in the northern part of the village, reaching 320 masl, directly adjacent to the Menoreh Mountains that extend to Magelang Regency. Figure 2 shows this highland area in red-yellow tones, located in the northeastern corner of Hargomulyo Area.

1.3. Landslide

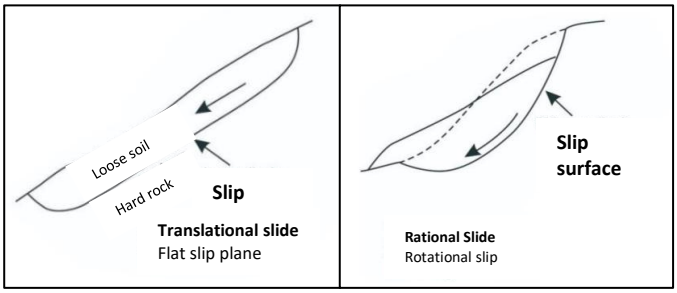

Figure 3. Illustration of the slip surface

A landslide is defined as the rapid and natural movement of a mass of soil, rock, or a mixture of both within a short period and over a large volume [24]. This phenomenon frequently occurs in hilly areas within tropical regions, where high rainfall intensity increases the likelihood of slope failure. Several physical processes such as soil movement, erosion, and water infiltration can trigger landslides [21], while slope steepness also plays a significant role. The impacts of landslides include changes in landform, loss of fertile

topsoil, and potential material damage or casualties [26]. On a broader scale, landslides may disrupt clean water systems, which can severely affect communities as clean water is a primary human necessity.

When a landslide occurs, the stability of the soil and slope materials becomes disturbed, commonly due to excessive rainfall or, in some cases, seismic vibrations. In steep hill slopes, the soil or rock mass moves downward along a slip surface — a layer that serves as the sliding plane for the landslide material [5]. Because the slip surface is impermeable, rainwater tends to accumulate above it, increasing pressure and eventually causing slope failure, as illustrated in Figure 3. The impermeable layer generally exhibits a distinct resistivity value compared to the permeable layer above it, which allows water infiltration. This difference forms the basis for identifying potential slip surfaces. Mapping these layers enables the investigation of landslide causes and helps assess future risk in the area.

1.4. Geoelectrical Method

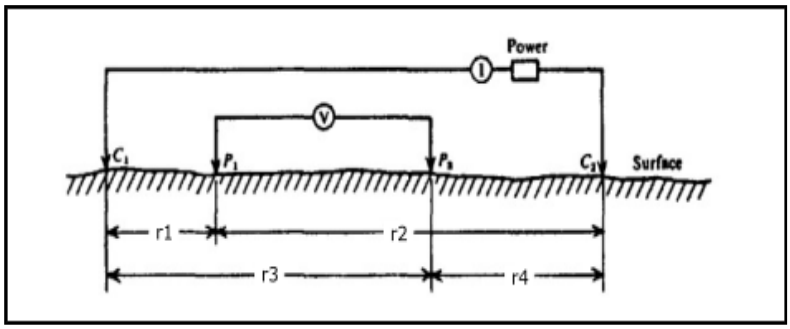

Figure 4. Two current and potential electrodes on the surface of a homogeneous medium [23]

The geoelectrical method is one of the main techniques in geophysics used to study how electric currents flow through the Earth and how these signals can be detected on or below the surface [22]. It aims to determine the distribution of subsurface resistivity by measuring electrical responses from the ground surface. This method is often preferred because it uses a controllable current source for data collection [23]. Each rock type has its own resistivity value, so by measuring resistivity, the type of subsurface material can be identified. This information is useful for understanding geological processes such as earthquakes or slope failures. In this method, a direct current (DC) is injected into the ground, and the resulting potential difference (ΔV) is measured to calculate apparent resistivity (ρ_a) using the equation [23]:

$$\rho_a = \frac{2\pi\Delta V}{I} \frac{1}{\left\{\left(\frac{1}{r_1}-\frac{1}{r_2}\right)-\left(\frac{1}{r_3}-\frac{1}{r_4}\right)\right\}} \quad (1)$$

where ρ_a is apparent resistivity, ΔV is potential difference, and I is the injected current, with r representing electrode spacing (see Figure 4). The geoelectrical resistivity method is widely applied in engineering geology for groundwater studies, geothermal exploration, identifying rock layers, and detecting soil contamination.

There are two main types of geoelectrical surveys: **Resistivity Sounding** and **Resistivity Mapping**. The Resistivity Sounding method, or Vertical Electric Sounding (VES), maps resistivity changes vertically by gradually increasing electrode spacing to reach deeper layers. The Schlumberger configuration is often used for this purpose [23]. It helps determine layer depth, structure, and resistivity, and is commonly applied in groundwater and mineral exploration. The **Resistivity Mapping** method, on the other hand, focuses on horizontal variations of resistivity to produce two-dimensional contour maps showing the distribution of subsurface materials. Wenner and Dipole–Dipole configurations are commonly used for this method, which is useful for identifying wide subsurface features such as mineral deposits or potential slip surfaces.

1.5. Wenner Configuration

During field data acquisition, the geoelectrical method employs several electrode configurations, each affecting the arrangement pattern and resulting geometric factor. Different electrode setups produce different geometric factors, and each configuration has its own specific purpose and advantages. One commonly used arrangement is the Wenner Configuration, first introduced by Frank Wenner in 1915.

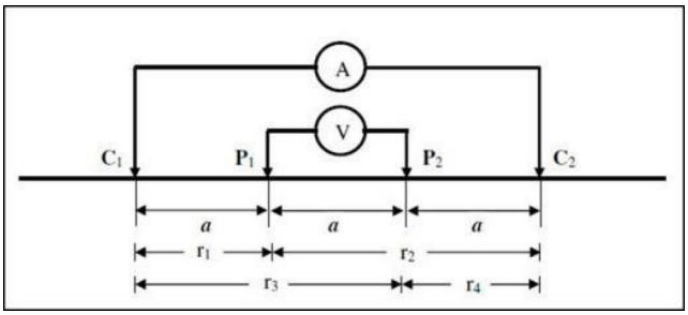

Figure 5. Electrode arrangement in the Wenner configuration [13]

In this configuration, the electrodes are arranged in a straight line symmetrically around a central point, with equal spacing between each electrode (Figure 5). The Wenner configuration provides good horizontal resolution and high lateral sensitivity but has limited current penetration depth [6]. Therefore, it is best suited for shallow subsurface mapping. The distance between adjacent electrodes is denoted as a, and the distance between the two current electrodes (C_1 and C_2) is three times the spacing between the potential electrodes (P_1 and P_2), or 3a. The geometric factor (K) for the Wenner configuration is expressed as [23]:

$$K = 2\pi a \quad (2)$$

1.6. Rock Resistivity

In simple terms, resistivity measurements are carried out by injecting an electric current through the current electrodes C_1 and C_2 (Figure 5), while the resulting potential difference is measured between the potential electrodes P_1 and P_2. Based on their ability to conduct electricity, materials are generally classified into three types: conductors, semiconductors, and insulators. Conductive materials have very low electrical resistance, while insulators have very high resistance. This resistance to electric current is what is measured as the resistivity of rocks.

It is often assumed that the Earth is a homogeneous and isotropic medium, meaning that the measured resistivity represents the true resistivity and does not depend on electrode spacing. However, in reality, the Earth is composed of multiple layers with varying resistivity values, causing the measured potential to be influenced by these layers. Rock resistivity measurements are affected by several factors, including rock homogeneity, water content, porosity, permeability, and mineral composition.

Table 1. Rock Resistivity Table [22]

Rock type	*Resistivity*(Ωm)
Porphyry (various)	$60 - 10^4$
Dacite	2×10^4 (wet)
Andesite	$4{,}5 \times 10^4$(wet) - $1{,}7 \times 10^2$ (*dry*)
Diabase (various)	$20 - 5 \times 10^7$
Schists (calcareous and mica)	10×10^4
Tuffs	2×10^3(wet) - 10^5 (*dry*)
Sandstones	$1 - 6{,}4 \times 10^8$
Limestones	$50 - 10^7$
Dolomite	$3{,}5 \times 10^2 - 5 \times 10^3$

Unconsolidated wet clay	20
Marls	$3 - 700$
Clays	$1 - 100$
Oil sands	$4 - 800$

2. METHODS

2.1. Data Acquisition

This research was conducted from February to September 2023. Field data acquisition took place in March and July 2023 in a landslide-prone area of Tangkisan 1, Hargomulyo, Kokap, Kulon Progo, Yogyakarta. The specific measurement site was on a hillside near the house of a local resident named Mr. Magi (399062 E, 9132771 S), where a landslide occurred on November 7, 2022. Although there were no casualties, the landslide damaged his garage and two parked motorcycles, as reported by detik.com on November 8, 2022 [3].

Data acquisition was carried out in three separate periods to optimize the research team's time and resources. The first period, on March 16–17, 2023, produced one profile named Line 2 (L2). The second period, from July 18–21, 2023, resulted in two profiles, Line 1 (L1) and Line 4 (L4). The final period, on July 28–29, 2023, produced Line 3 (L3). The intervals between each period were used for data processing and verification of previously collected data.

According to the Geological Map of Yogyakarta Sheet [16], the study area lies within an andesite intrusion formation. Topographically, it is located on a hillside with the ridge at an elevation of approximately 210 meters above sea level, based on the DEMNAS map obtained from tanahair.indonesia.go.id. The slope is densely vegetated with trees, although some parts have been cultivated with crops such as cassava and banana. The equipment used for data acquisition included a Naniura geoelectrical resistivity meter set from the Physics Laboratory of UIN Sunan Kalijaga Yogyakarta, along with electrodes, cables, a 12V battery, a multimeter, and supporting tools for fieldwork.

2.2. Data Processing

The collected data were processed using Microsoft Excel. Based on Ohm's Law, the resistance (R) was calculated, followed by determining the geometric factor (K) and the apparent resistivity (ρa). The coordinates and elevation of each electrode position were also recorded to support the modeling process.

Once the apparent resistivity values were obtained, the data were formatted for processing in Res2Dinv software. The organized data were saved as a text file (.txt) and imported into Res2Dinv x64 ver 4.10 to generate a two-dimensional subsurface resistivity model. Topographic data were also included to enhance the accuracy of the model and to assist in interpreting the geological features observed in the field.

The next step was slip surface analysis, which aimed to identify the layer that potentially acts as a failure plane based on resistivity values. This analysis was supported by field observations and reference data from previous studies to ensure accurate layer classification.

The final model was a classified 2D representation of the subsurface, with each color indicating different rock or soil layers. For instance, bedrock was shown in yellow, the slip surface in green, and potentially unstable material in blue. This visualization provided a clearer understanding of the subsurface structure and the potential zones of instability.

3. RESULTS AND DISCUSSION

3.1. Line 1

The modeling results from Res2Dinv for Line 1 (L1) are shown in Appendix Figure 6. Line 1 extends for 300 meters, with the highest elevation at 221 meters above sea level located at point L1-T25, and the lowest at 190 meters at point L1-T275. The deepest modeled layer reaches 142 meters above sea level at point L1-T160, approximately 61 meters below the highest surface elevation.

The surface soil layer, represented in blue, has a resistivity value of 54.5 Ωm. This layer is found in several areas, such as between L1-T40 and L1-T150 at depths greater than 10 meters. It is overlain by a mixture of clay and weathered andesite (green) and andesite (yellow) layers. The surface soil layer also

appears between L1-T120 to L1-T230 and L1-T240 to L1-T270, each having a thickness of more than 10 meters from the surface.

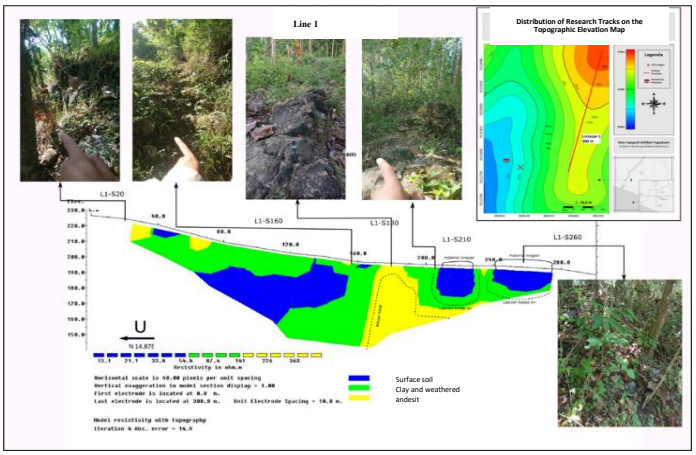

Figure 6. 2D model of subsurface rocks along Line 1

The clay and weathered andesite layer, with resistivity values ranging from 54.5 Ωm to 141 Ωm, is also observed in multiple sections. At L1-T140, it forms a thin layer beneath the bedrock. It reappears between L1-T55 and L1-T85, about 10 meters thick, overlain by a thin andesite layer. Another section is found between L1-T75 and L1-T130, about 20 meters thick, and extends southward from L1-T130 to L1-T160, reaching a maximum depth of nearly 60 meters at an elevation of 145 meters above sea level. This layer reappears between L1-T185 and L1-T210, about 25 meters thick, and resurfaces between L1-T230 and L1-T240. It is represented by the green color in the 2D model.

The andesite bedrock layer, with resistivity values ranging from 141 Ωm to over 363 Ωm, is represented by the yellow color in the model. This layer is identified in various parts of the profile, such as between L1-T25 and L1-T40, with a thickness of about 10 meters down to an elevation of 210 meters. A more extensive andesite layer is found between L1-T165 and L1-T195, at depths from 20 to 40 meters, surfacing again at L1-T180. Several minor bedrock layers are also observed at L1-T70, L1-T150, and L1-T235. This classification is supported by field observations, where outcrops were found at points L1-S155, L1-S180, and L1-S230.

3.2. Line 2

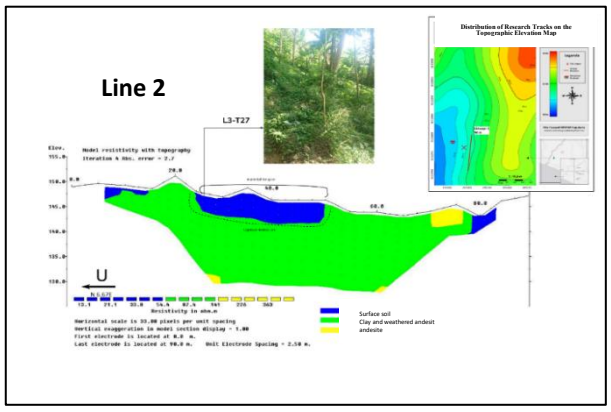

Figure 7. 2D model of subsurface rocks along Line 2

Line 2 (L2) extends for 90 meters, with the highest elevation located at L2-T20 at 150 meters above sea level, and the lowest point at L2-T65 with an elevation of 142.5 meters. The maximum depth reached in this 2D model is approximately 23 meters from the highest surface point, or 127.5 meters above sea level. The modeled section spans from L2-T7 to L2-T83 (Figure 7). This line is positioned above the previous slope failure area that occurred on November 8, 2022, as mentioned earlier. During field measurements, the surface

along this line consisted of a grass-covered footpath, with some portions planted with cassava and banana trees.

The 2D model (Figure 7) indicates that most of the subsurface along Line 2 consists of a layer with resistivity values ranging from 54.4 Ωm to 141 Ωm. This layer is interpreted as a mixture of clay and weathered andesite, which is likely to serve as the slip surface in the study area. The surface soil material, represented in blue, has resistivity values between <13.1 Ωm and 54.4 Ωm. It appears between L2-T5 and L2-T15 with a thickness of about 2.5 meters, and reappears between L2-T25 and L2-T50, reaching up to 4 meters thick and extending to the lowest elevation of 142 meters above sea level.

The andesite bedrock layer, shown in yellow, has resistivity values from 141 Ωm to over 363 Ωm. This layer is identified between L2-T70 and L2-T80, with a thickness of approximately 4 meters. Bedrock is also detected at a depth of 17.5 meters from the surface near L2-T25, and reappears at L2-T60, at a depth of 20 meters or an elevation of 127.5 meters above sea level.

3.3. Line 3

Line 3 (L3) extends for 150 meters, with the 2D model spanning from L3-T13 to L3-T137. The highest elevation along this line is 128 meters above sea level at L3-T13, while the lowest point is 120 meters above sea level at L3-T137. The maximum depth reached in this model is approximately 33 meters from the highest surface point, or 95 meters above sea level (Figure 8).

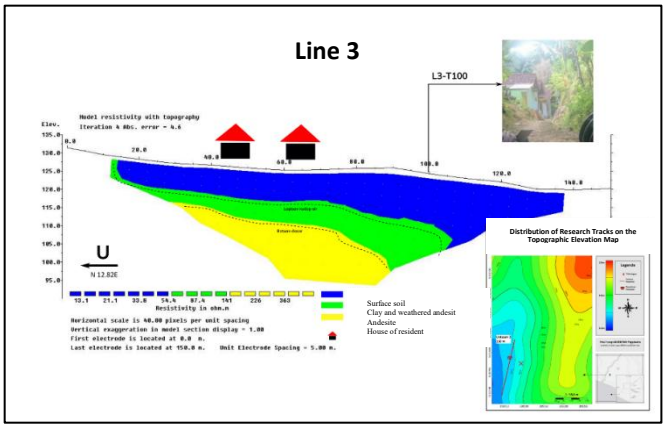

Figure 8.2D model of subsurface rocks along Line 3

As in the previous lines, the 2D model was interpreted based on resistivity values, color codes, and rock types. The surface soil layer, represented in blue, is distributed almost continuously along the entire line (Figure 8) It begins near L3-T15 with a thickness of about 5 meters and extends to L3-T135. The thickest part of this layer is found around L3-T115, where it reaches up to 27 meters.

Beneath it lies a layer interpreted as a mixture of clay and weathered andesite. This layer appears at the surface around L3-T15, extends beneath the topsoil, and ends near L3-T100 at a depth of 15 meters (approximately 105 meters above sea level). The thickest portion of this layer occurs at L3-T90, with an estimated thickness of 15 meters.

The andesite bedrock layer, represented in yellow (Figure 8), lies directly below the potentially unstable soil and the slip surface layer. It first appears at L3-T30 at a depth of 10 meters (around 116 meters above sea level) and extends to L3-T90. Based on the model, the andesite layer exceeds 15 meters in thickness, reaching down to an elevation of approximately 95 meters above sea level.

3.4. Track 4

Line 4 (L4) has a different orientation compared to the previous three lines, extending 225 meters from west to east along an uphill slope. The lowest point is located at L4-T0 with an elevation of 115 meters above sea level, while the highest point is at L4-T225, reaching 193 meters above sea level. The 2D model for this line extends from L4-T17 to L4-T202 (Figure 9), with a maximum modeled depth of 103 meters relative to the highest point at L4-T225, or approximately 90 meters above sea level.

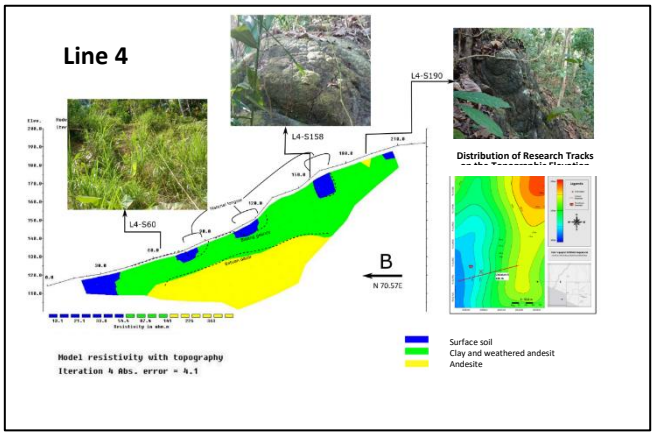

Figure 9. 2D model of subsurface rocks along Line 4

Based on the model (Figure 9), the andesite bedrock has resistivity values ranging from 141 Ωm to more than 363 Ωm. It is found at depths greater than 10 meters below the slope surface. More specifically, the bedrock appears at L4-T50 at a depth of 15 meters (around 110 meters above sea level) and continues to L4-T165 at a depth exceeding 22 meters (around 140 meters above sea level). Additional andesite layers are also observed near L4-T195.

Above the bedrock lies a mixture of clay and weathered andesite, extending almost continuously from L4-T30 to L4-T210. This layer has a thickness ranging from 15 meters on the lower slope (around L4-T60) to 30 meters near L4-T160. Overlying this, though not evenly distributed, is a surface soil layer, represented in blue on the model. It appears at L4-T30 with a thickness of 10 meters, at L4-T75 (7 meters), between L4-T85 and L4-T120 (7 meters), around L4-T165 (12 meters), and again at the end of the model at L4-T210 with a thickness of 5 meters.

3.5. Geological Correlation and Interpretation of Slip Surface

The interpretation of the subsurface models is consistent with the geological framework presented in the *Geological Map of Yogyakarta Sheet* [16]. The study area is primarily composed of the *Andesite Intrusion* and the *Kebobutak Formation*. The *Andesite Intrusion*, consisting of hypersthene–andesite to trachyandesite, occupies the northern and central portions of Hargomulyo, while the *Kebobutak Formation*, composed of alternating andesitic breccia, tuff, and lava flows, dominates the surrounding hills.

High-resistivity zones exceeding 141 Ωm observed across all profiles correspond to intact andesite bedrock belonging to the intrusive unit. This layer is relatively impermeable and mechanically competent, acting as the foundation of the slope. In contrast, the intermediate-resistivity zones ranging from 54.4 to 141 Ωm are interpreted as weathered andesite mixed with clay. This layer represents a weathering zone developed along the lithological contact between the *Andesite Intrusion* and the volcaniclastic rocks of the *Kebobutak Formation*. The alteration process within this boundary zone produces clay minerals and weakens the material's shear strength, allowing it to function as a potential slip surface.

The presence of this clay–weathered andesite layer beneath the surface soil in L1 to L4 confirms that the potential slip surface is lithologically controlled, forming along the transition from the weak, weathered zone to the underlying intact andesite. Additionally, a local fault trending north–south through Hargomulyo may enhance groundwater infiltration along fractures, thereby increasing pore-water pressure above the impermeable bedrock. This mechanism explains why landslides are recurrent in the area, particularly during periods of intense rainfall.

Overall, the resistivity interpretation not only delineates the position of the slip surface but also clarifies its geological context within the existing formations and structures. These findings strengthen the understanding that slope instability in Hargomulyo is governed by lithological contrasts, weathering intensity, and local structural conditions within the andesitic terrain.

4. CONCLUSION

Based on the resistivity modeling and geological correlation, the layer identified as the potential slip surface consists of clay mixed with weathered andesite, showing resistivity values between 54.4 and 141 Ωm. This weak zone is consistently observed in all four survey lines at depths of 0 to 20 meters below the surface. The underlying layer with resistivity values exceeding 141 Ωm represents intact andesite bedrock belonging to the Andesite Intrusion unit, which forms a mechanically stable foundation.

The slip surface is lithologically controlled, forming along the transition between the weathered andesite–clay layer and the impermeable andesite bedrock. This interpretation aligns with the geological conditions of the Hargomulyo area, where the contact between the Andesite Intrusion and the Kebobutak Formation produces a weathered zone prone to failure. The presence of a local fault may also enhance water infiltration, increasing pore pressure and triggering slope movement during heavy rainfall.

These findings highlight the importance of integrating resistivity data with geological mapping to improve the identification of potential landslide zones. The results of this study can serve as a reference for slope stability assessment and landslide mitigation efforts in similar andesitic terrains across Kulon Progo and surrounding regions.

DECLARATION

Author Contribution

Both authors contributed equally to the conception, design, data analysis, and writing of the manuscript.

Funding

This study received no external funding and was entirely financed by the researchers.

Acknowledgments

The authors would like to thank all parties who supported the completion of this research, including colleagues and institutions involved in data collection and analysis.

Conflict of Interest

The authors declare no conflict of interest.

REFERENCES

[1] H. Amir, Akmam, Bavitra, and M. Azhari, “Penentuan Kedalaman Batuan Dasar Menggunakan Metode Geolistrik Resistivitas dengan Membandingkan Konfigurasi Dipole-Dipole dan Wenner di Bukit Apit Puhun Kecamatan Guguk Panjang Kota Bukittinggi,” Eksakta, vol. 18, no. 2, pp. 19–31, 2017. [Online]. Available: http://eksakta.ppj.unp.ac.id

[2] Badan Informasi Geospasial, Peta Topografi Wilayah Yogyakarta, 2018. [Online]. Available: https://tanahair.indonesia.go.id/demnas/#/#Info

[3] J. R. Dewantara, “Tebing 15 Meter di Kokap Kulon Progo Longsor, Rumah dan Motor Tertimbun,” Detik.com, 2022. [Online]. Available: https://www.detik.com/jateng/jogja/d-6394078/tebing-15-meter-di-kokap-kulon-progo-longsor-rumah-dan-motor-tertimbun

[4] R. F. Erviani, Sutarto, and Indrawati, “Model Pembelajaran Instruction, Doing dan Evaluating (MPIDE) Disertai Resume dan Video Fenomena Alam dalam Pembelajaran Fisika di SMA,” Jurnal Pembelajaran Fisika, vol. 5, pp. 53–59, 2016.

[5] G. Fatmawati, S. Gussri, and Afdal, “Investigasi Bidang Gelincir Tanah Longsor Menggunakan Metode Geolistrik Resistivitas 2 Dimensi Konfigurasi Wenner (Studi Kasus: Padayo Bukit Atas Indarung Kecamatan Lubuk Kilangan Kota Padang),” Jurnal Fisika Unand, vol. 11, no. 4, pp. 487–493, 2022. [Online]. Available: http://jfu.fmipa.unand.ac.id/index.php/jfu/article/view/941

[6] Hakim and R. H. Manrulu, “Aplikasi Konfigurasi Wenner dalam Menganalisis Jenis Material Bawah Permukaan,” Jurnal Ilmiah Pendidikan Fisika “Al-Biruni”, vol. 5, pp. 95–103, 2016.

[8] A. Harjanto, “Vulkanostratigrafi di Daerah Kulon Progo dan Sekitarnya, Daerah Istimewa Yogyakarta,” Magister Teknik Geologi, vol. 4, no. 8, pp. 4–18, 2011.

[9] Jufriyanto, Perhitungan Cadangan Mangan dari Survei Metode Polarisasi Terinduksi di Desa Karangsari Kecamatan Pengasih Kabupaten Kulonprogo Daerah Istimewa Yogyakarta, Undergraduate Thesis, Department of Physics, Faculty of Science and Technology, UIN Sunan Kalijaga, Yogyakarta, 2017.
[10] D. Lesmana, M. Fauzi, and B. Sujatmoko, "Analisis Kemiringan Lereng Daerah Aliran Sungai Kampar dengan Titik Keluaran Waduk PLTA Koto," Jom FTEKNIK, no. 8, pp. 1–7, 2021.
[11] M. Muiz, Pendugaan Bidang Gelincir Tanah Longsor Berdasarkan Sifat Kelistrikan Bumi dengan Metode Geolistrik Konfigurasi Wenner: Studi Kasus Area Rawan Longsor Desa Mertelu Kecamatan Gedangsari Kabupaten Gunungkidul, Undergraduate Thesis, Department of Physics, Faculty of Science and Technology, UIN Sunan Kalijaga, Yogyakarta, 2016.
[12] Munaji, S. Imam, and I. Lutfinur, "Penentuan Resistivitas Batuan Andesit Menggunakan Metode Geolistrik Konfigurasi Schlumberger (Studi Kasus Desa Polosiri)," Jurnal Fisika, vol. 3, no. 2, pp. 117–121, 2013.
[13] R. R. Pambudi, M. Nurul, W. P. Prihadita, and R. Mulyasari, "Analisis Kelongsoran dengan Metode Geolistrik Konfigurasi Wenner-Schlumberger dan Wenner-Alpha di Jalan Raya Suban Bandar Lampung," Jurnal GeoCelebes, pp. 108–116, 2022.
[14] R. Prastowo, "Pemodelan 2D Resistivitas Batuan Andesit Daerah Gunung Kukusan Kulon Progo," Kurvatek, vol. 2, no. 2, pp. 87–93, 2017.
[15] E. B. Purwasatriya, "Dinamika Rekayasa," vol. 9, no. 2, pp. 54–60, 2013.
[16] W. Rahardjo, Sukandarrumidi, and H. M. D. Rosidi, Peta Geologi Lembar Yogyakarta, Jawa. Bandung: Pusat Penelitian dan Pengembangan Geologi, 1995.
[17] S. Hidayatullah, A. B. Santoso, and R. Prastowo, "Penerapan Metode Kriging pada Pemodelan Andesit Menggunakan Data Geolistrik Daerah Gunung Kali Songgo Kulon Progo," Prosiding Nasional Rekayasa Teknologi Industri dan Informasi XIII, pp. 89–95, 2018.
[18] I. Suardi, P. Ariyanto, K. Nafi, S. Ariwibowo, and M. Ali, "Identifikasi Bidang Gelincir Menggunakan Metode Resistivitas Konfigurasi Wenner (Studi Kasus Dusun Sijeruk, Kabupaten Banjarnegara)," Prosiding Seminar Nasional Fisika dan Aplikasinya, pp. 61–68, 2019.
[19] Sulaiman, Identifikasi Bidang Gelincir Tanah Menggunakan Metode Geolistrik Konfigurasi Wenner: Studi Kasus Area Rawan Longsor Desa Selopamioro, Kec. Imogiri, Kab. Bantul, Undergraduate Thesis, Department of Physics, Faculty of Science and Technology, UIN Sunan Kalijaga, Yogyakarta, 2016.
[20] M. A. Syam, R. I. Putri, and A. I. Rambe, "Interpretasi Bidang Gelincir Longsoran Tanah Menggunakan Metode Geolistrik Konfigurasi Wenner di Sungai Pinang, Kota Samarinda, Provinsi Kalimantan Timur," Prosiding Nasional Rekayasa Teknologi Industri dan Informasi XVII, pp. 641–645, 2022.
[21] M. Syukri, Dasar-Dasar Metode Geolistrik. Banda Aceh: Syiah Kuala University Press, 2020.
[22] W. M. Telford, L. P. Geldart, and R. E. Sheriff, Applied Geophysics, 2nd ed. New York: Cambridge University Press, 1990.
[23] Uca and R. Maru, Mitigasi Bencana: Pemetaan dan Zonasi Daerah Rawan Longsor dan Banjir. Malang: Media Nusa Creative, 2019.
[24] S. C. Wahyono, K. G. Atmadja, and S. S. Siregar, "Identification of Andesite Rock Based on the Resistivity Value in Satui Area, South Kalimantan," JGE (Jurnal Geofisika Eksplorasi), vol. 6, no. 3, pp. 173–182, 2020.
[25] A. P. Wicaksono, N. Y. Rahmatussadah, U. Prabowo, and O. Trianda, "Investigasi Bidang Gelincir Pemicu Gerakan Tanah (Tanah Longsor) dengan Metode Geolistrik di Desa Sambirejo, Kecamatan Prambanan, Kabupaten Sleman," Prosiding Nasional Rekayasa Teknologi Industri dan Informasi XVI, pp. 433–444, 2021.